

## **Ion Conduction Mechanism in Solid Polymer Electrolyte: An Applicability of Almond-West Formalism**

Namrata Shukla<sup>1,\*</sup>, Awalendra K. Thakur<sup>2</sup>, Archana Shukla<sup>3</sup>, David T. Marx<sup>1</sup>

<sup>1</sup> Department of Physics, Illinois State University, Normal, Illinois, 61790, USA.,

<sup>2</sup> Department of Physics, Indian Institute of Technology (IIT), Patna, Bihar - 800013, India

<sup>3</sup> Department of Metallurgical Engineering & Material Science, Indian Institute of Technology Bombay Mumbai, -400076, India,

\*E-mail: [ntripat@ilstu.edu](mailto:ntripat@ilstu.edu)

Received: 17 July 2014 / Accepted: 25 September 2014 / Published: 28 October 2014

---

Dielectric response and ac conductivity analysis of an ionically conducting polymer film based on polymethyl methacrylate (PMMA) as the host polymer have been carried out. The effect of frequency and salt concentration on the dielectric relaxation and on the ac conductivity has been observed. The dielectric behavior was analyzed via the dielectric permittivity ( $\epsilon'$ ) and dissipation factor ( $\tan \delta$ ) of the samples. The analysis has shown the presence space charge polarization at lower frequencies. Evidences of dielectric and conductive relaxation phenomena have also been traced. The dielectric peak has been observed to shift toward the higher frequency side with the addition of LiClO<sub>4</sub> salt, suggesting a lowering the sample viscosity and the barrier to ion mobility. The real part of ac conductivity spectra of these materials obeys the Jonscher power law, where the calculated value of the power law exponent  $n$  lies between 0.5 and 1, which confirms that the electrical conductivity in the polymer nanocomposite electrolytes (PNCs) is primarily due to ionic transport. The hopping rate, carrier concentration term, has been determined using Almond-West formalism. A good correlation among dielectric permittivity, carrier concentration and ionic conductivity has been observed.

---

**Keywords:** polymers; electron microscopy; dielectric properties; electrical conductivity, ac conductivity

### **1. INTRODUCTION**

Solid polymer electrolytes formed by the distribution of alkali metal salts in polymers have been receiving great attention recently due to their application in high-energy electrochemical devices [1-3]. The advantages of these materials are their light weight, flexibility, ability to form intricate shapes, and low manufacturing cost [4, 5]. Various polymers such as PEO [6-8], PMMA [9], PAN [10, 11], and PVDF [12] have been studied with these advantages in mind. Obtaining high conductivity at

ambient temperature is the main goal in order for these materials to be used in electrochemical applications. For over three decades, researchers have sought these high conductivity polymers, but so far, conductivity of more than  $10^{-3}$  S cm<sup>-1</sup> has not been achieved. The main hurdle in achieving this goal is an incomplete understanding of the conduction mechanism in polymer electrolytes [13-14].

The conductivity of this polymer electrolyte depends on the molecular mobility and charge transport. Many recent studies have been carried out [15–18] involving neutron scattering, nuclear magnetic resonance (NMR), X-ray diffraction (XRD), and computer simulation to investigate the ion transport process. Dielectric properties (dielectric permittivity and dielectric loss) also constitute a powerful source for obtaining information about the characteristics of ionic and molecular interaction. Dielectric relaxation is of particular significance in ionic conductivity, and the dielectric constant is a measure of reduction of Coulomb interaction, and hence plays a fundamental role in the ability of polymer to dissolve salt. Frequency-dependent conductivity and dielectric relaxation both are sensitive to the motion of charged species and the dipoles of the polymer electrolyte. Thus, these studies provide important information on the ionic transport mechanism of fast ion conductors [19, 20].

The ac conductivity ( $\sigma_{ac}$ ) measurements also provide considerable information on ion dynamics and conductivity relaxation, when  $\sigma_{ac}$  results are expressed as a function of frequency. The electrical transport (conductivity), in an ion conducting polymeric system, is determined by factors like concentration of the charge carriers and the rate at which they are mobile (hopping) from one available site to another. There should be complete information on both factors in order to understand the mechanism of conduction. Based on applicability of Jonscher's universal power law (Eq. 1), Almond and West [21] developed a formalism, to evaluate carrier concentration term  $K$  (Eq 2). The equations are

$$\sigma(\omega) = \sigma_{dc} + A\omega^n \quad (1)$$

$$K = \frac{\sigma_{dc}T}{\omega_p} \quad (2)$$

where,  $\sigma_{dc}$ ,  $A$ ,  $n$ , and  $T$  are the dc conductivity, pre-exponential factor, fractional exponent and temperature, respectively.

In this context, the present work was carried out to explore ion dynamics in polymethyl methacrylate (PMMA)–LiClO<sub>4</sub>-based polymer electrolytes using frequency-dependent dielectric relaxation and conductivity.

## 2. EXPERIMENTAL

### 2.1 Material Preparation

Polymer electrolyte films were prepared using the standard solution cast technique with PMMA (Aldrich, MW:  $2 \times 10^5$ ) as the polymer host matrix and LiClO<sub>4</sub> (Acros Organics, USA) as the salt for complexation. The polymer host (PMMA) was vacuum dried and the salt (LiClO<sub>4</sub>) was dried at 150 °C for 24 h to remove surface adsorbed moisture prior to sample preparation. An appropriate stoichiometric ratio of PMMA was dissolved in acetonitrile (Merck) and the solution was stirred for 12

h. Subsequently, a calculated amount of  $\text{LiClO}_4$  was added and stirred for 12 h to facilitate homogeneous mixing and complexation. In the final polymer-salt complex solution for each salt concentration, the solvent was allowed to evaporate slowly at room temperature ( $27^\circ\text{C}$ ). The dried free standing polymer salt complex (PS) films were then vacuum dried at  $40^\circ\text{C}$  to remove any residual solvent before storing them in an inert medium until further analysis.

## 2.2 Materials Characterization

The morphological and surface properties of the PS films were studied using an electron microscope (SEM JOEL-JSM Model5800). Dielectric measurements on the composite films were carried out in the frequency range of 0.1 Hz to 100 kHz using a computer-interfaced impedance analyzer (HIOKI LCR Hi-Tester Model 3532, Japan). The samples were placed in a cell configuration of  $\text{SS} | \text{PS} | \text{SS}$ , where SS stands for stainless steel blocking electrodes and PS is the polymer-salt complex. A 200-mV ac signal of was applied across the cell and the temperature was cycled as measurements were taken. The complex impedance spectroscopy (CIS) spectra are reproducible on cooling, thus we deduce that there is no water remaining in the sample that would influence the conductivity of the samples.

## 3. RESULTS AND DISCUSSION

### 3.1 Scanning Electron Microscopy

Figure 1 shows scanning electron micrographs of PMMA and PS films. The PMMA image shows smooth morphology with appreciable micro-pores.

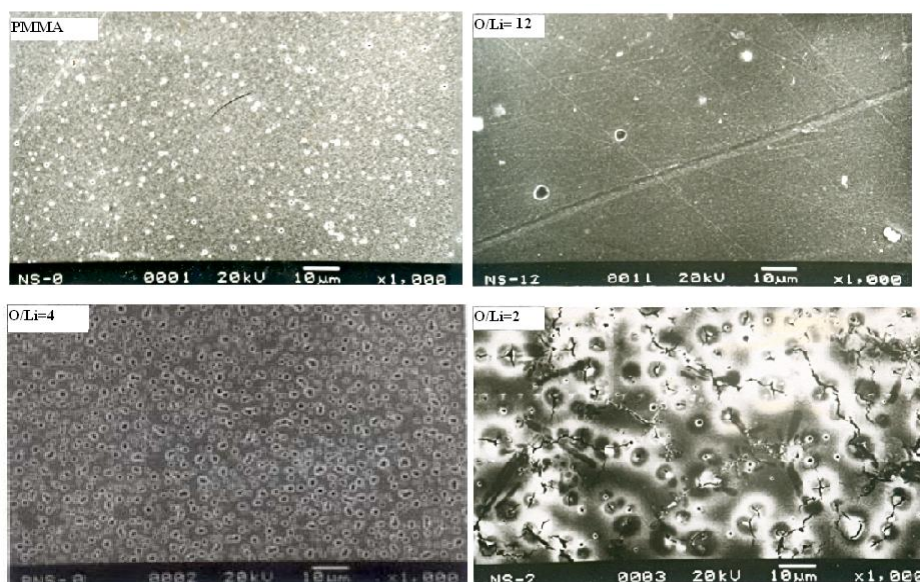


**Figure 1.** Scanning electron micrographs (SEM images) of PMMA and PMMA- $\text{LiClO}_4$  films with  $\text{O/Li} = 12, 4, \text{ and } 2$ .

The smooth morphology is closely related to the amorphous nature of the polymer. The small pores are caused by the fast evaporation of the solvent (acetonitrile) during the sample preparation process. A clear modification in surface morphology of pure PMMA takes place on addition of the salt. On addition of even a small amount of salt (O/Li ~ 12, i.e., 8 wt%), the image shows an irregular wavelike appearance due to polymer–salt complex formation. The pore size increases with further addition of salt, and the PS film with O/Li = 4 shows a porous structure with uniform pore distribution at the microscopic level. At higher salt concentration (O/Li ~ 2, i.e., 35 wt%), some fine streaks and cracks begin to develop on the rough surface, showing the appearance of crystalline texture in the sample.

### 3.2 Analysis of Electrical Properties

#### 3.2.1 Complex Impedance Spectroscopy (CIS) Analysis

The CIS pattern of the polymer-salt complex samples for selected salt concentrations at  $T \sim 30$  °C and at 100 °C are shown in Figure 2, along with their equivalent electrical circuit representations (as inset).

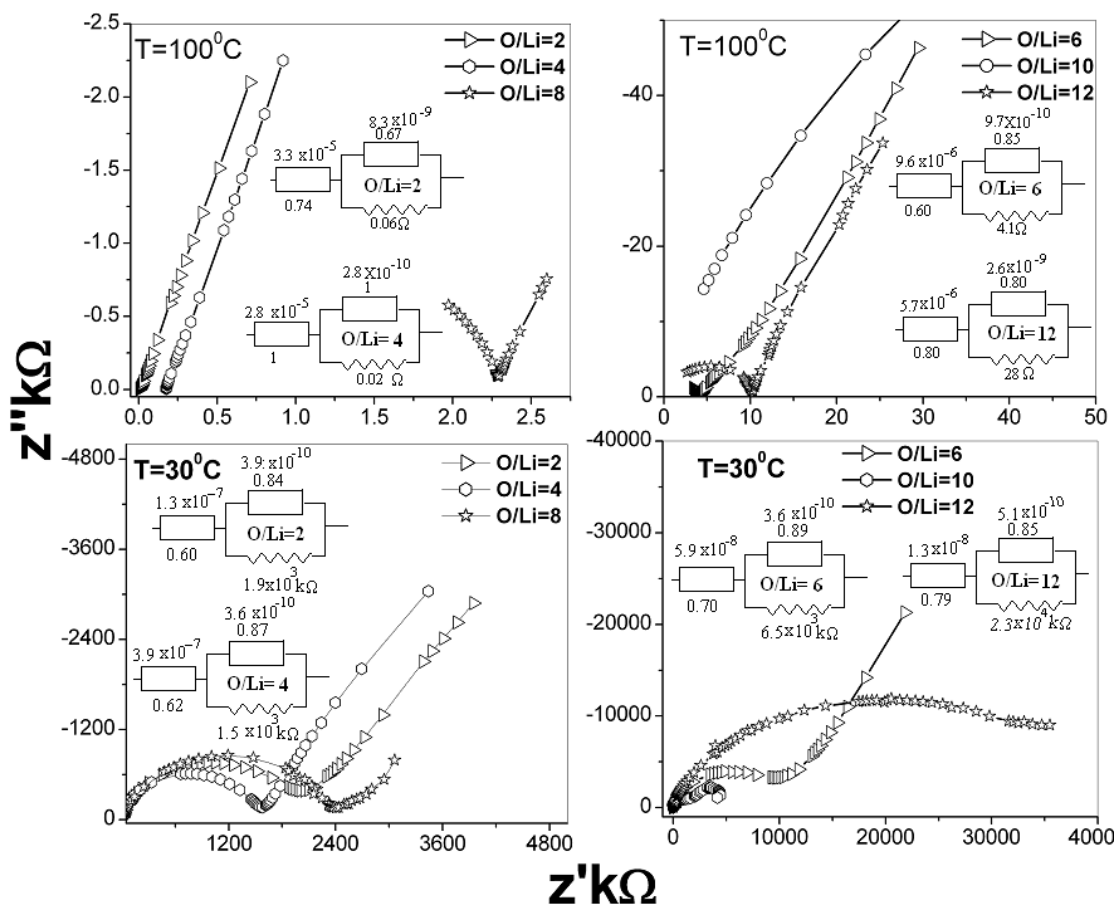


Figure 2. Impedance plot for PMMA-LiClO<sub>4</sub> with different O/Li ratio at 30 °C and at 100 °C

The complex impedance plots at both temperatures show a high frequency arc followed by a low frequency spike that may be related, respectively, to the bulk conduction process and the accumulation of charges at the electrolyte–electrode (blocking electrode) interface, which is commonly referred to as the double layer capacitive effect ( $C_{dl}$ ) [22]. At both the temperatures (30 and 100 °C), the electrical equivalent circuit modeling of all the PS films consists of a parallel combination of resistance ( $R$ ) and the constant phase element (CPE) in series combination with another CPE. The CPE values of bulk samples are less than the film CPE values due to interfacial polarization. The fit chi-squared values lie between  $10^{-4}$ - $10^{-5}$ , which suggests good NLLS fit.

The presence of the CPE in the equivalent electrical circuit model is due to the deviation from ideal CIS response; i.e., the flattening/deformation in the semicircular arc. The deviation is due to inhomogeneity in the local distribution of defects near phase boundaries, the distribution of relaxation times, and current and potential distributions associated with electrode geometry [23] as well as forward-backward jumps of ions in the polymer matrix [24]. The impedance of the CPE ( $Z_{CPE}$ ) is normally represented as:  $Z_{CPE} = \frac{1}{Q_0(J\omega)^n}$ , where  $Q_0$  and  $n$  are fitting parameters such that it may

behave as an electrical analogue of resistance, Warburg impedance, capacitance, and inductance corresponding to different values of  $n$ : 0, 0.5, 1, and  $-1$ , respectively. The dimension of CPE is  $\Omega^{-1}\cdot S^n$ , whereas that of capacitance is  $\Omega^{-1}\cdot S$ . For  $n < 1$ , the magnitude of capacitance can be calculated as  $C = Q\omega_{max}^{(n-1)}$  [25]. At 30 °C, the PS film with O/Li = 4 shows the highest value of double layer capacitance ( $C_{dl} \sim 10^{-7}$   $\mu F$ ) and lowest value of bulk resistance ( $R_b \sim 1.5$  M $\Omega$ ). The high value of  $C_{dl}$  results from the large charge accumulation at the electrode–electrolyte interface. At 100 °C, the electrical equivalent circuit remains the same, but with different CPE and  $R$  values. At this temperature, the highest value of  $C_{dl}$  ( $1.3 \times 10^{-5}$   $\mu F$ ) and lowest value of bulk resistance (0.06 k $\Omega$ ) are found for the O/Li = 2 PS film. For this PS film, the bulk resistance is 3-4 orders of magnitude smaller as compared to its room temperature value. On the other hand, the double layer capacitance values of PS films at 100 °C are 2 orders of magnitude higher than those at room temperature. This increase in  $C_{dl}$  value is due to a higher dissociation of salt, and the decrease in  $R$  value is due to faster ion dynamics at higher temperature.

At both temperatures (RT & 100 °C), the conductivity increases on addition of salt. The highest conductivities,  $\sim 6.7 \times 10^{-9}$  S cm $^{-1}$  and  $\sim 7.2 \times 10^{-5}$  S cm $^{-1}$  at RT and 100 °C, respectively, are observed for O/Li  $\sim 4$  (21% salt w.r.t. PMMA w/w). The dramatic enhancement in the value of conductivity at 100 °C may be directly related to polymer chain flexibility above the glass transition ( $T \geq T_g \sim 95$  °C) as well as to the property of the amorphous polymer electrolyte to provide a larger free volume with increasing temperature, which facilitates ion migration and causes an increase in ionic conductivity [26, 27].

### 3.2.2 Dielectric Analysis

Figure 3 shows the variation of real part of the permittivity ( $\epsilon'$ ) and dielectric loss ( $\tan \delta$ ) with varying salt concentration as a function of frequency at room temperature (30 °C). For salt

concentrations indicated by O/Li = 2, 4, and 8, the permittivity pattern exhibits two distinct dispersive regions, characterized by a change in slope.

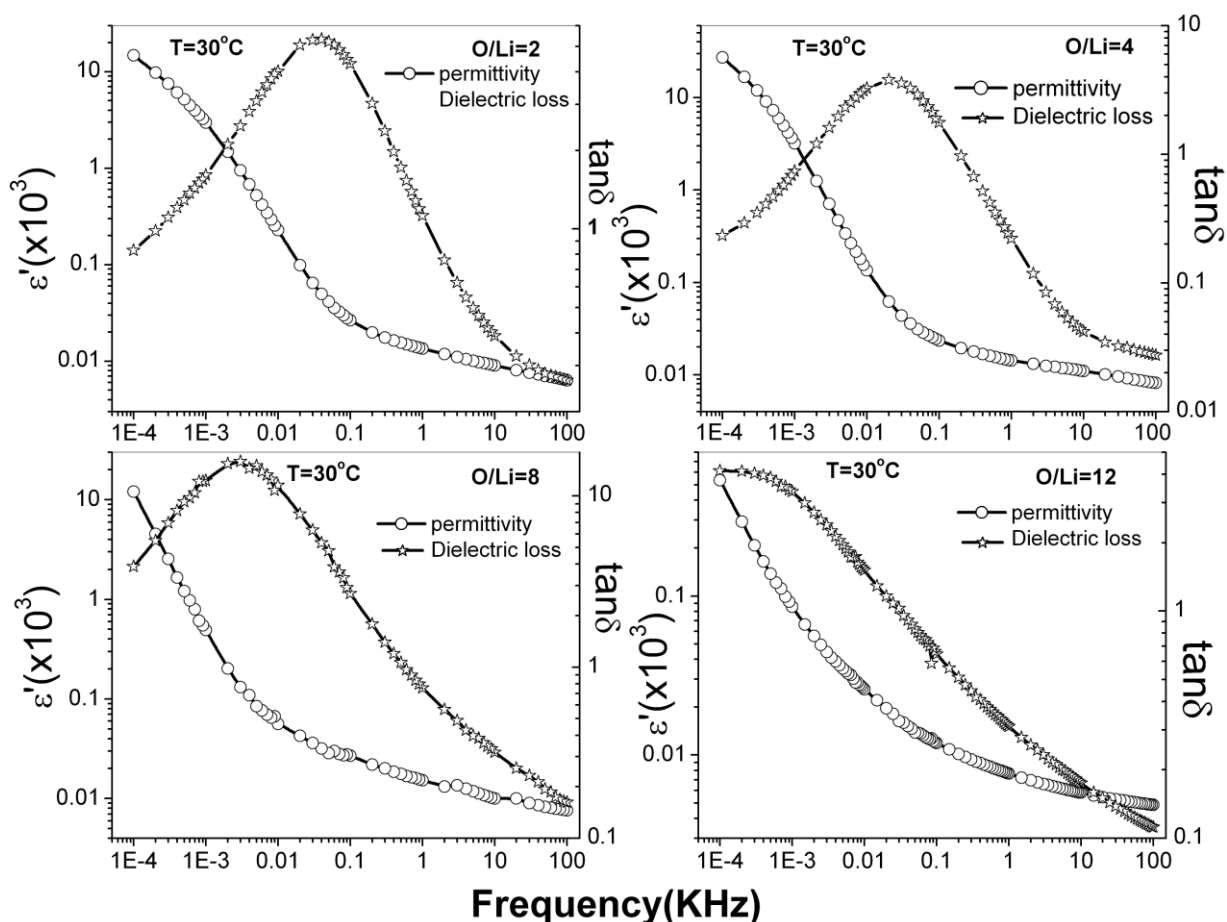


**Figure 3.** Variation of dielectric loss and permittivity as a function of frequency for different polymer to cation ratios at 30 °C

The pattern of changes in slope varies with salt concentration in the PS. For the low frequency dispersive region, the dielectric constant increases sharply followed by a progressive decrease in its magnitude in the higher frequency dispersive region. As the salt concentration increases, the frequency at which the dispersion becomes prominent shifts towards higher frequency side. A typical result indicates that with an increase in the salt concentration from 12 wt% (O/Li=8) to 21 wt% (O/Li = 4) of PMMA (w/w), the dielectric constant shows a corresponding increase. However, any further increase in the salt concentration (from O/Li = 4 to O/Li = 2) does not significantly change the magnitude of dielectric constant. The high frequency dispersive region shows similar behavior to the low frequency dispersion region.

The dielectric loss ( $\tan \delta$ ) for the PS films shows a typical peak for each salt concentration. These peaks appear at the same frequency at which the crossover (change in frequency) occurs in the permittivity pattern. With increase in the salt concentration, the magnitude of the loss decreases and the loss peak shifts towards higher frequency. The asymmetric loss ( $\tan \delta$ ) peak around the maximum

frequency ( $\omega_{\max}$ ) suggests a deviation from classical exponential Debye behavior. The full width half maxima (FWHM) values of the  $\tan \delta$  peaks are also found to be broader than the ideal Debye peak. The FWHM would be equal to 1.14 decades for a Debye process representing the bulk properties of the material. The angular frequency of the applied field  $\omega$ , at which the  $(\tan \delta)_{\max}$  occurs, defines the relaxation time,  $\tau=1/2\pi f_{\max}$ .

At 30 °C, the low frequency dispersive region is due to charge accumulation at the electrode electrolyte interface [28] and the high frequency dispersive region may be related to the hopping of charge carriers from one available site to another in the host polymer matrix. These hopping charge carriers behave like dipoles. The observed space charge in the low frequency region can be explained in terms of ion diffusion [29] governed by  $\omega^{(n-1)}$ -type variation referred to as non-Debye type behavior [30]. On addition of the salt, the dielectric constant increases dramatically, and its value at 50 Hz is given in Table 1. An increase in the dielectric constant with salt concentration increase is most likely due to accumulation of higher number of charge carriers at the electrode-electrolyte interface. This increase in dielectric constant with increase in salt concentration is attributed to a fractional increase in charges within the polymer electrolyte (PS) matrix. The dependence of charge carrier concentration ( $n$ ) on the dissociation energy ( $U$ ) and dielectric constant ( $\epsilon$ ) is given in the following equation [31].

$$n = n_0 e^{-U/\epsilon k_{\beta} T} \quad (3)$$

where  $k_{\beta}$  is the Boltzmann constant and  $T$  is the absolute temperature.

**Table 1.** Dielectric constant and loss of PMMA-LiClO<sub>4</sub> films at 30 °C and 100 °C

Salt Ratio: O/Li	T = 30 °C		T = 100 °C	
	Dielectric permittivity (50 Hz)	Dielectric Loss	Dielectric permittivity	Dielectric Loss (tan $\delta$ )
PMMA	3.6	0.06	-----	-----
12	13.8	0.84	$2.4 \times 10^3$	5.5
8	28.6	4.8	$3.6 \times 10^4$	2.6
4	31.4	7.7	$7.0 \times 10^6$	0.0
2	41.4	5.2	$1.2 \times 10^6$	0.4

The dielectric constant increases with increasing salt concentration up to O/Li = 4. This increase in dielectric constant indicates that there is an increase in the number of charge carriers (from Eq. 3), which results in the increased conductivity [32]. The value of ( $\epsilon'$ ) decreases as the frequency is increased due to the high periodic reversal of the field at the interface that, in turn, reduces the contribution of the charge carriers. At 100 °C, the dielectric constant in the high frequency region increases due to the faster ion dynamics and higher dissociation of salt at the higher temperature.

Dielectric loss is a direct measurement of the energy dissipated and generally arises from ionic transport and charge polarization. The accumulation of charges at the electrode-electrolyte interface results in the formation of macro dipoles that oscillate with the frequency of applied field. These charge accumulations exhibit relaxation behavior similar to dipolar relaxation [33]. Hence, the

accumulated ionic charges in a PS matrix are also expected to exhibit a polarization peak in the dielectric loss spectra as shown in the frequency vs. dielectric loss pattern [Figure 3] for all salt concentrations (O/Li = 2 to 12). Since the dielectric loss peak is in the near dc frequency range (mHz to a few Hz), these losses may be attributed to conduction. The rapid decrease in the loss accompanied by the corresponding rapid increase in the  $\epsilon'$  also confirms this reasoning. The overall effect causes enhanced interfacial polarization [33-36]. The  $\tan \delta$  peak shifts toward higher frequencies with increasing salt concentration, thereby reducing the relaxation time. It causes a corresponding increase in the dielectric constant that may be attributed to the presence of a larger fraction of ionic species in the PS matrix.

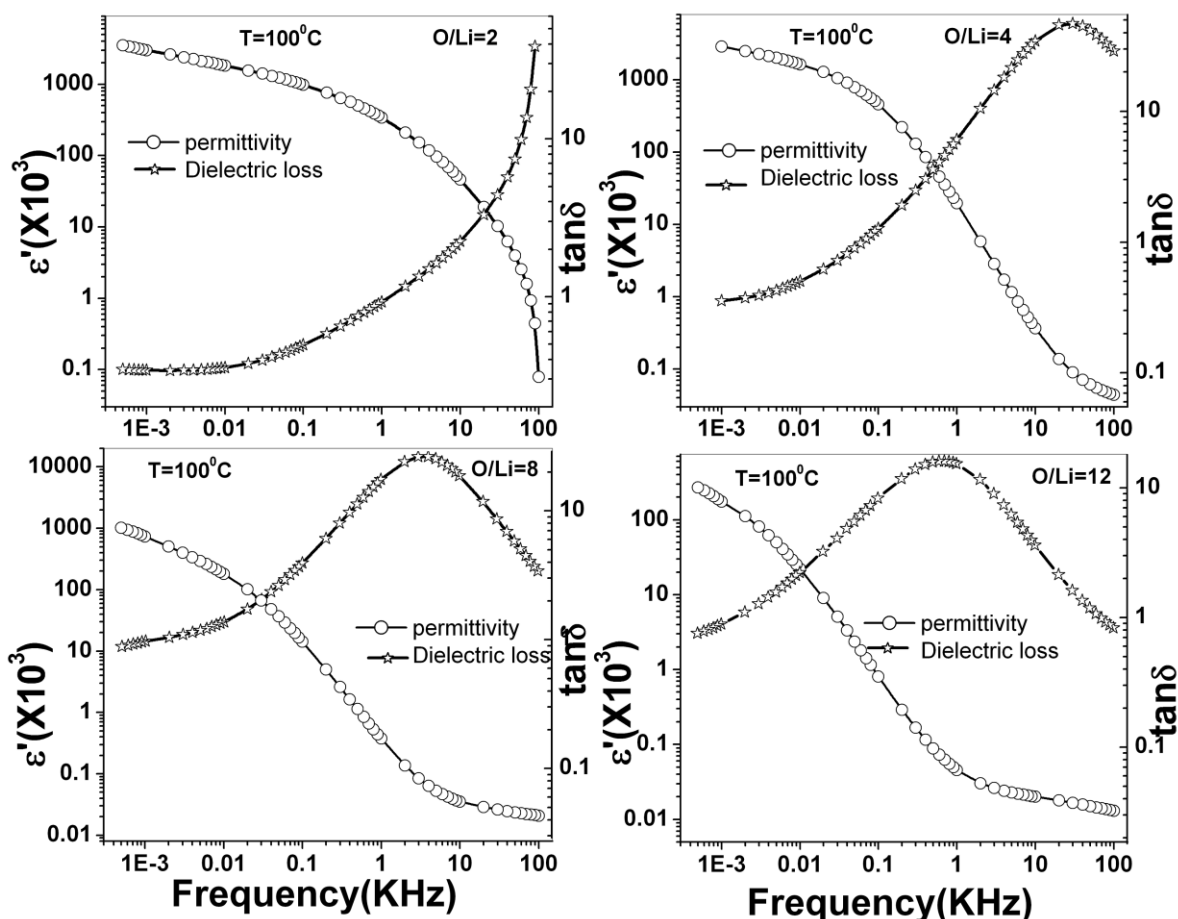


**Figure 4.** Variation of dielectric loss and permittivity as a function of frequency for different polymer to cation ratios at 100 °C

The interaction of the Li<sup>+</sup> ion with the C=O electronegative group of PMMA makes the side chain bulky that causes an increase in the main chain-chain separation and a corresponding decrease in glass transition temperature ( $T_g$ ). Hence, an increase in the flexibility of the host polymer backbone with increasing salt concentration facilitates the ionic motion, which is governed by charge carrier interaction (ion-ion) and ion-polymer interactions. Figure 4 shows the variation of the real part of permittivity ( $\epsilon'$ ) and tangent loss with varying salt concentration as a function of frequency at 100 °C, which is near the glass transition temperature. The permittivity at 100 °C exhibits three distinct

behavior regions: a low frequency saturation region is followed by intermediate and high frequency dispersive regions. The dielectric loss and ( $\epsilon'$ ) behavior with increasing salt concentration are very similar to that at RT with the essential difference being in the magnitudes of the permittivity and loss. The permittivity value is higher in comparison to that at 30 °C, and the loss peak is observed at higher frequency. While the electrode polarization phenomenon is more pronounced in the low and intermediate frequency regions, the high frequency dispersive behavior is attributed to the combined effect of ionic and dipolar polarization.

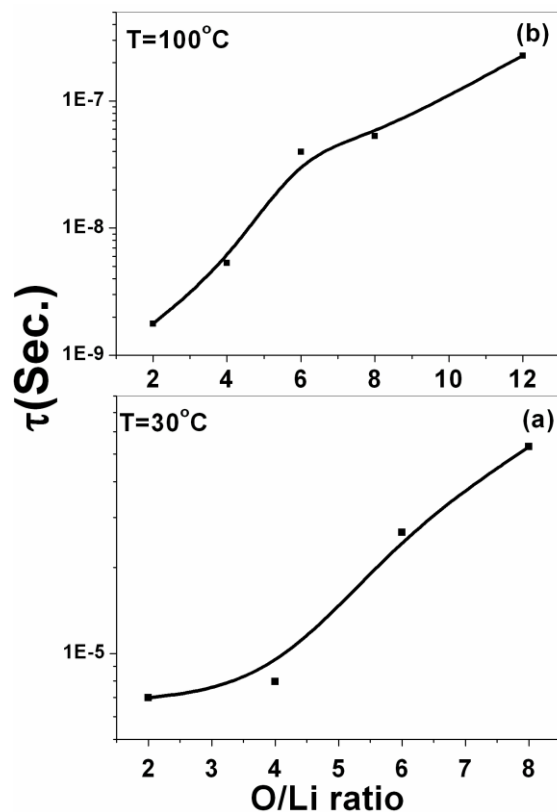


**Figure 5.** Variation of relaxation time as a function of salt concentration at (a) 30 °C and (b) 100 °C

As a consequence, the dielectric constant increases with increasing salt concentration and results in an increase in ionic conductivity. The larger value of dielectric constant at higher temperature may be related to the higher dissociation of salt at high temperatures [37]. The relaxation peaks for all salt concentrations at 100 °C exhibit a shift toward higher frequency in comparison to the 30 °C values. This is to the result of faster ion dynamics at high temperature. As a result, the charge carrier concentration as well as the mobility of charge carriers increases. Since the ionic conductivity of a solid polymer electrolyte (SPE) is

$$\sigma = \sum_i n_i z_i \mu_i \tag{4}$$

where  $n$ ,  $z$  and  $\mu$  represent the charge carrier concentration, charge of mobile carrier, and the mobility, respectively, the conductivity at high temperature should be higher than at RT. An increase

in charge carrier concentration with salt addition at elevated temperatures seems reasonable in view of the expected dissociation of ion-pairs under thermal activation.

This interpretation also seems consistent with the observed variation of the relaxation time ( $\tau$ ) with salt concentration shown in Figures 5a and 5b. The variation in relaxation time with salt concentration at 30 °C and at 100 °C is shown, and the data shows that the relaxation time decreases with increasing salt concentration. Hence, an increase in conductivity with increasing salt concentration is a likely possibility up to a limiting concentration. At 30 °C, the PS sample with O/Li = 4 shows the smallest relaxation time ( $\sim 7 \times 10^{-3}$  s), which is consistent with its higher conductivity. At high temperature (100 °C), a three orders of magnitude decrease is observed in the relaxation time. Hence, the conductivity for all samples is greater than the room temperature values due to faster ion transport.

### 3.2.3 Ac conductivity analysis

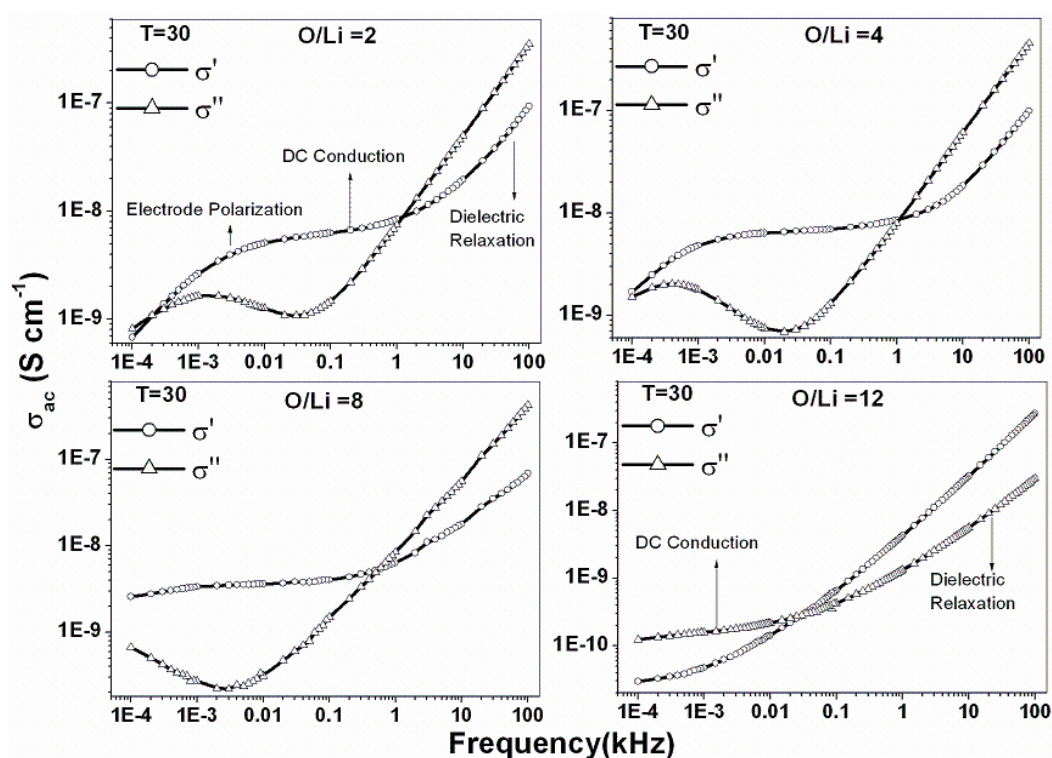


**Figure 6.** Variation of  $\sigma'$  &  $\sigma''$  as a function of frequency for different polymer to cation ratios at 30 °C

Figures 6 and 7 show the variation of conductivity  $\sigma'$  and  $\sigma''$  with frequency at 30 °C and 100 °C. At 30 °C, the conductivity spectrum for the sample with low salt concentration (O/Li = 12), consists of two frequency regions: (i) a frequency-independent zone in the mHz range and (ii) a regime of power law increase in conductivity at higher frequencies. A similar trend in frequency-dependent conductivity is reported in the literature for ionically conducting ceramic glasses and polymers [38-40]. For the same samples, the  $\sigma''$  frequency response shows two regions recorded as a low frequency-independent region followed by a frequency-dependent region. The low frequency-independent region

for  $\sigma'$  is due to the dc conductivity contribution while the high frequency behavior represents a bulk relaxation phenomenon.

At higher salt concentrations ( $O/Li = 2, O/Li = 4$ ), the frequency-dependent conductivity exhibits three regions: (i) a low frequency dispersive region, (ii) a mid frequency saturation region, and (iii) a high frequency dispersive region. With an increase in salt concentration, the  $\sigma'$  frequency response shows a shift in the frequency dispersive region as well as in the frequency-dependent region towards the higher frequencies. For low salt concentrations ( $O/Li = 12, O/Li = 8$ ), the low frequency dispersive region falls outside the measured frequency range, hence it could not be observed. A peak in the  $\sigma''$  response vs. frequency accompanies the low frequency dependent region of  $\sigma'$ . This is attributed to the electrode polarization effect.

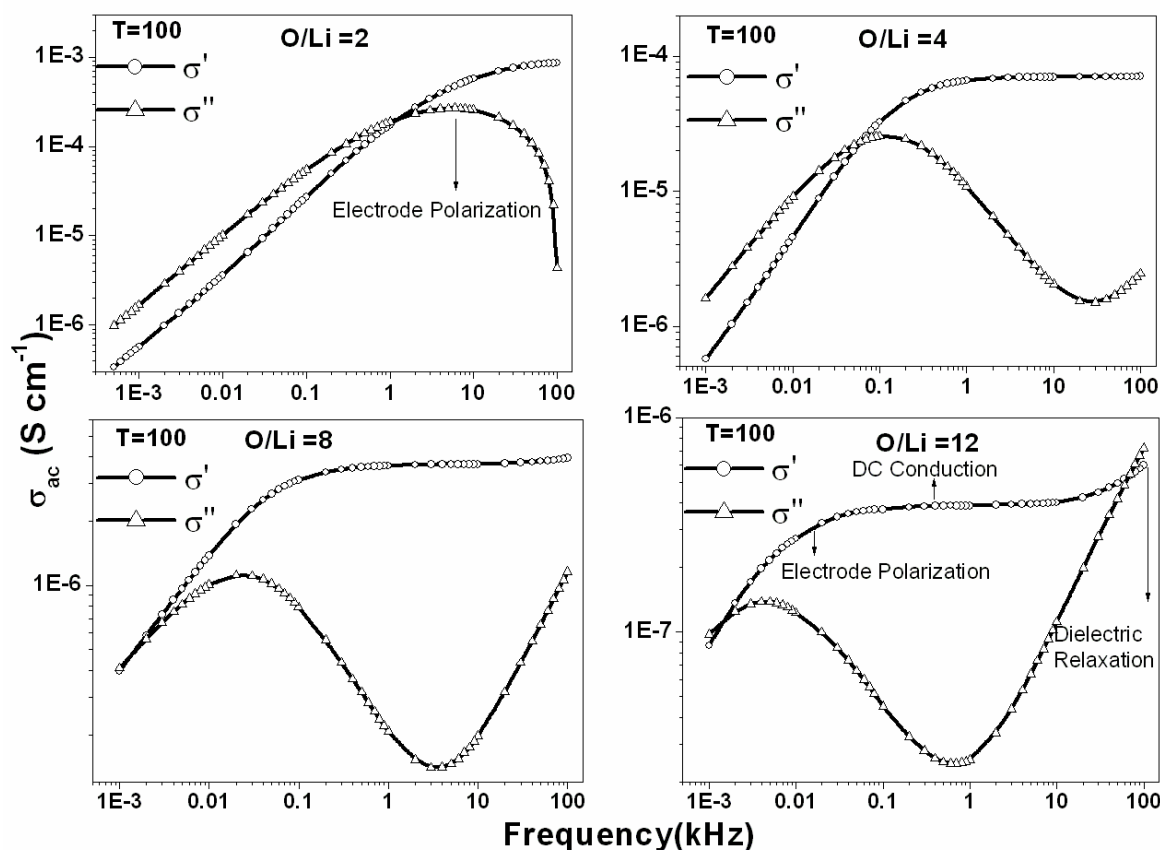


**Figure 7.** Variation of  $\sigma'$  &  $\sigma''$  as a function of frequency for different polymer to cation ratios at 100 °C

The conductivity decreases with decreasing frequency in the low frequency-dependent region. This decrease in conductivity may be due to the accumulation of more charges at the electrode-electrolyte interface at low frequency, which causes the decrease in the number of mobile ions. The slope of the low frequency dispersion curve varies with salt concentration at both 30 °C and 100 °C. This is due to varying strength of interfacial polarization effect. For the same sample at both temperatures, the low frequency dispersion in the ac conductivity versus frequency response and the permittivity vs. frequency response lie in almost the same frequency range. In the high frequency

region, both  $\sigma'$  and  $\sigma''$  increase with increasing frequency, primarily due to the dielectric contribution [37]. For the PS with low salt concentration ( $O/Li = 12,8$ ) at  $100\text{ }^\circ\text{C}$ , all three regions exist, whereas for high salt concentration ( $O/Li = 4, 2$ ), the high frequency region falls outside the range of the measurement. This behavior of the conductivity follows Jonscher's universal power law (Eq. 1) [41].

At lower frequencies, ions travel much faster and are able to jump from one available site ( $C=O$ ) to another in the host polymer matrix. An ion successfully hops to a vacant neighboring site due to the long relaxation time and contributes to the dc conductivity. A successful hop occurs when the frequency is lower than the hopping frequency ( $\omega_p$ ).

At higher frequencies, two competing relaxation processes may be visualized: (i) the jumping ion to jumps back to its initial position (correlated forward-backward-forward), i.e., unsuccessful hopping and (ii) the neighborhood ions become relaxed with respect to the ion's position (the ions stay in the new site), i.e., successful hopping. The increase in the ratio of successful to unsuccessful hopping results in a more dispersive conductivity at higher frequencies [42]. Such ionic motion occurs when the frequency exceeds  $\omega_p$ , which is characteristic frequency corresponding to the onset of conductivity dispersion [43]. When frequency exceeds  $\omega_p$ ,  $\sigma'$  increases proportionally on, where  $n < 1$ . Jonscher's power law fits for the experimental results are shown in Figures 8 and 9. The chi-squared value of fit lies between  $10^{-13}$  and  $10^{-14}$ , which suggests a very good Jonscher power law fit. The saturation limit in the low frequency region gives an estimate of  $\sigma_{dc}$ , whereas the frequency-dependent region fitting provides an estimate of the pre-exponential factor ( $A$ ) and fractional exponent ( $n$ ). The carrier-hopping rate was determined using the Almond and West method[44] and the carrier concentration term ( $K$ ) has been calculated using Eq (2). The experimentally determined values of these parameters are shown in Table 2.

From Table 2, it is clear that the value of  $n$  lies between 1 and 0.5. This confirms that our SPE system is predominantly an ionic conductor. The carrier-hopping rate and carrier concentration term increase with the salt concentration, and a corresponding increase in conductivity is observed.

**Table 2.** Values for the fractional exponent, pre-exponential factor, ion hopping rate and carrier concentration at 30 and  $100\text{ }^\circ\text{C}$ .

O/Li	$T = 30\text{ }^\circ\text{C}$				$T = 100\text{ }^\circ\text{C}$			
	$n$	$A$	$\omega_p$ (kHz)	$K$ ( $\Omega^{-1}\cdot\text{cm}^{-1}\cdot\text{H}$ $\text{z}^{-1}\text{ }^\circ\text{C}$ )	$n$	$A$	$\omega_p$ (kHz)	$K$ ( $\Omega^{-1}\cdot\text{cm}^{-1}\cdot\text{H}$ $\text{z}^{-1}\text{ }^\circ\text{C}$ )
2	0.75	$3.7 \times 10^{-10}$	18.3	$1 \times 10^{-11}$	---	---	---	---
4	0.83	$1.3 \times 10^{-10}$	18.1	$1.2 \times 10^{-11}$	---	---	---	---
8	0.62	$1.6 \times 10^{-9}$	4.3	$2.1 \times 10^{-11}$	0.71	$2 \times 10^{-9}$	186.3	$1.9 \times 10^{-9}$
12	0.78	$1.4 \times 10^{-10}$	1.4	$2.8 \times 10^{-12}$	0.65	$5.2 \times 10^{-11}$	119.8	$3.2 \times 10^{-10}$
15	0.75	$1.5 \times 10^{-10}$	0.3	$6.9 \times 10^{-13}$	0.62	$9.3 \times 10^{-10}$	0.8	$1.0 \times 10^{-10}$

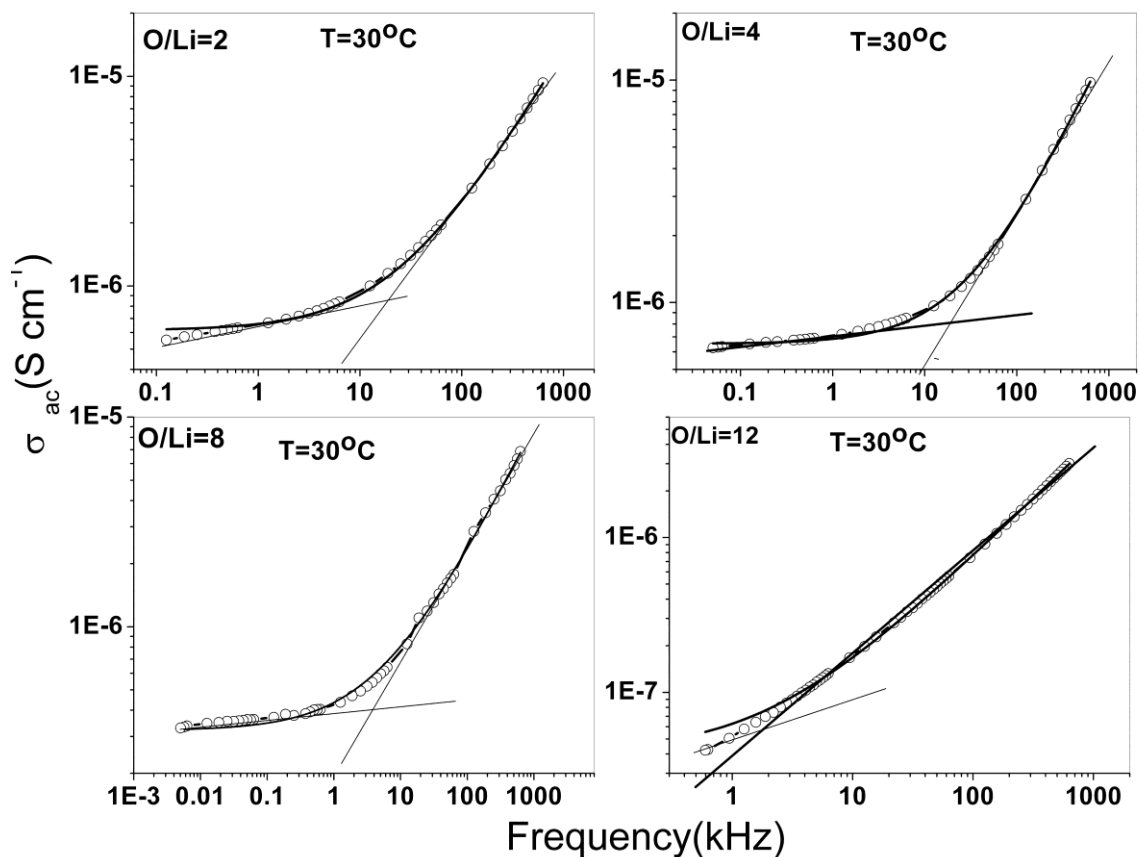


**Figure 8.** Jonscher power law fitting of ac conductivity at 30°C

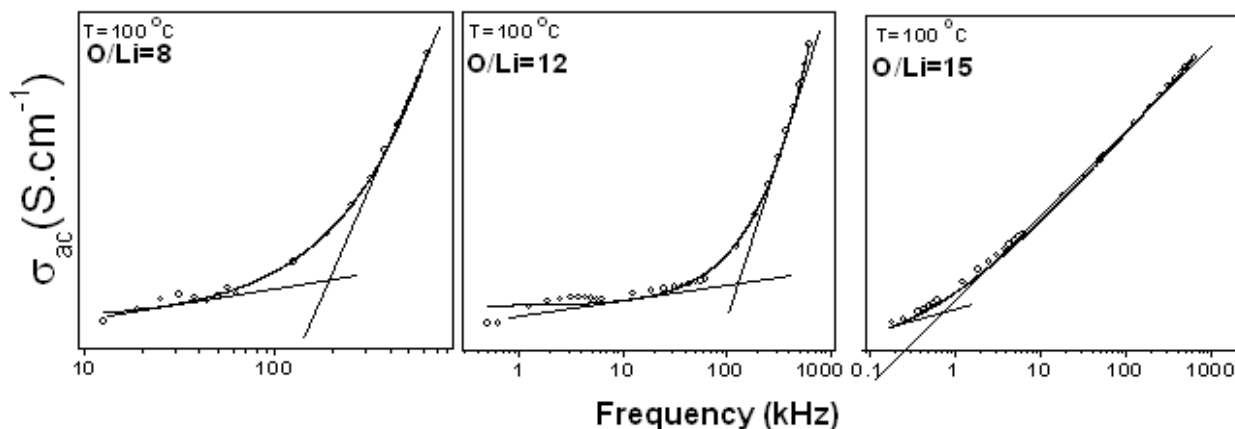


**Figure 9.** Jonscher power law fitting of ac conductivity at 100°C

For a particular sample, the carrier concentration term at 100 °C is higher in comparison to that at 30 °C. Hence, for all samples, the ionic conductivity is also higher at 100 °C. The variation of dielectric constant, carrier concentration and conductivity with salt concentration at 30 °C is shown in Figure 10.

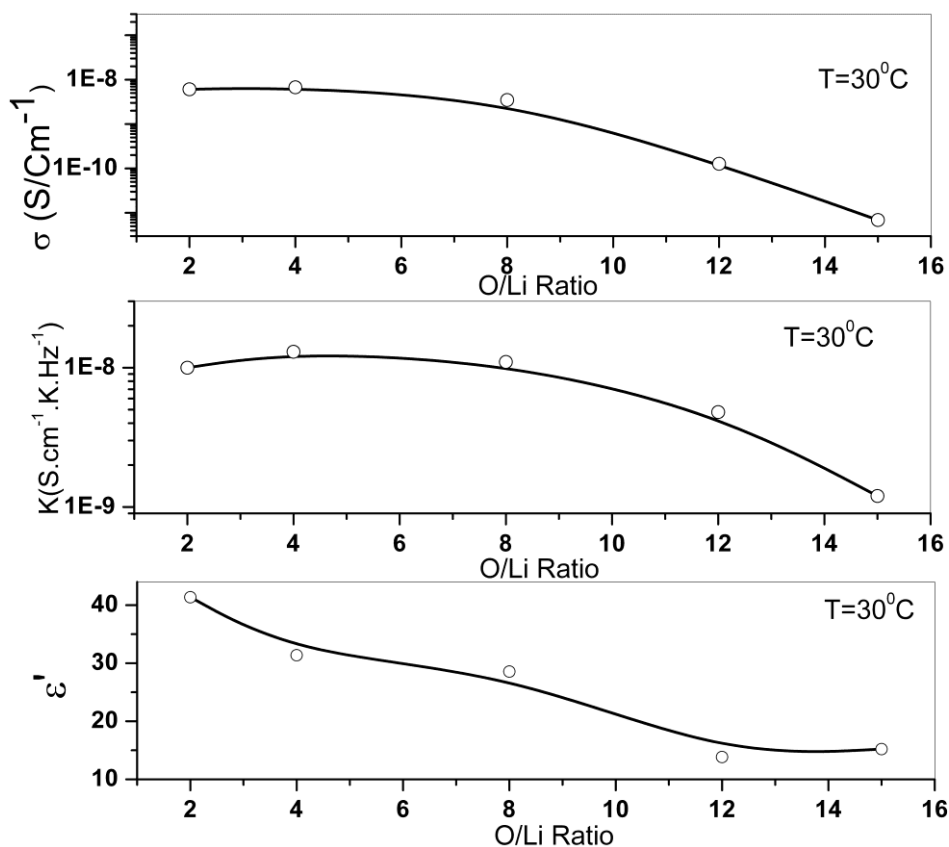


**Figure 10.** Variation of dielectric constant, mobile carrier concentration and dc conductivity as a function of salt concentration.

A very good correspondence among the variation of conductivity, carrier concentration and dielectric permittivity with salt concentration clearly suggests that the origin of dielectric behavior lies in the conducting species and their interaction. So, an increase in dielectric constant depends on the number of charge carriers in the host polymer matrix.

#### 4. CONCLUSIONS

Polymer electrolyte films have been prepared by solution cast technique. The dielectric behavior of the films has been analyzed in terms of frequency response of dielectric permittivity ( $\epsilon'$ ) and dissipation factor ( $\tan \delta$ ). Such an analysis has confirmed the presence of electrode polarization effects due to space charge polarization at lower frequencies. The appearance of the loss peak in the low frequency (mHz to a few Hz) region is attributed to the losses due to dc conduction. The real part of ac conductivity spectra of the materials obeys Jonscher power law at higher frequency whereas dispersion in lower frequency confirms the presence of the electrode polarization effect. It has been observed that an increase of salt concentration reduces the ionic conductivity relaxation time, and hence, increases ionic conductivity. A correlation between ion hopping rate ( $\omega_p$ ) and the carrier

concentration term ( $K$ ) has been determined from the experimental results. The analysis appears to be consistent with the observed variations in conductivity.

#### ACKNOWLEDGEMENT

One of the authors acknowledges with thanks the financial support received from the Council of Scientific and Industrial Research (CSIR), Government of India, New Delhi for carrying out the research at the Department of Physics, Indian Institute of Delhi (IITD), Hauz Khas, New Delhi 110016, India.

#### References

1. B. Scrosati (Ed.), *Applications of Electroactive Polymers*, Chapman and Hall, London (1993).
2. F. M. Gray (Ed.), *Solid Polymer Electrolytes—Fundamentals and Technological Applications*, VCH, New York (1991).
3. M. Watanabe, K. Sanui, N. Ogata, T. Kobayashi and Z. Ohtaki, *J. Appl. Phys.* 57 (1985) 123.
4. J. Xi, X. Qiu, S. Zheng and X. Tang, *Polymer* 46 (2005) 5702.
5. P. G. Bruce, *Solid state electrochemistry*, Cambridge University Press, Cambridge (1995).
6. C. J. Leo, G. V. Subba Rao and B. V. R. Chowdari, *Solid State Ionics* 148 (2002) 159.
7. S. R. Mohapatra, A. K. Thakur and R. N. P. Choudhary, *J. Power Sources* 191 (2009) 601.
8. D. K. Pradhan, R. N. P. Choudhary and B. K. Samantray, *Int. J. Electrochem. Sci.* 3 (2008) 597.
9. N. Shukla and A. K. Thakur, *J. Non-Crystalline Solids* 15 (2011) 4236.
10. Y. W. Chen-Yang, H. C. Chen, F. J. Lin and C. C. Chen, *Solid State Ionics* 150 (2002) 327.
11. A. L. Sharma, N. Shukla and A. K. Thakur, *J. Poly. Sci.: Part B: Poly. Phys.* 46 (2008) 2577.
12. A. Magistris, E. Quartarone, P. Mustarelli, Y. Saito and H. Kataok, *Solid State Ionics* 152 (2002) 347.
13. D. E. Fenton, J. M. Parker and P. V. Wright, *Polymer* 14 (1973) 589.
14. C. A. Angell, C. Lin and E. Sanchez, *Nature* 362 (1993) 137.
15. G. Mao, R. F. Perea, W. S. Howells, D. L. Price and M. L. Saboungi, *Nature* 405 (2000) 163.
16. B. Wang, S. Q. Li and S. J. Wang, *Phys. Rev. B* 56 (1997) 11503.
17. P. Mustarelli, C. Capiglia, E. Quartarone, C. Tomasi, P. Ferloni and L. Linati, *Phys. Rev. B* 60 (1999) 7228.
18. G. S. MacGlashan, Y. G. Andreev and P. G. Bruce, *Nature* 398 (1999) 792.
19. B. Rolling, *J. Non-Crystalline Solids* 244 (1999) 34.
20. S.R. Mohapatra, A.K. Thakur and T. Sakuma, *J. Phys. Soc. Jpn.* 79 (2010) Suppl. A 169.
21. D. P. Almond and A. R. West, *Solid State Ionics* 9-10, (1983) 277.
22. C. Kim, G. Lee, K. Lio, K. S. Rhu, O. S. G. Kang and S. H. Chang, *Solid State Ionics* 123(1999) 251.
23. M. R. Shoar Abouzari, F. Berkemeier, G. Schmitz, D. Wilmer, *Solid State Ionics* 180 (2009) 922.
24. H. W. Chen, T. P. Lin and F. C. Chang, *Polymer* 43 (2002) 5281.
25. C.S. Hsu and F. Mansfeld, *Corrosion* 57 (2001) 747.
26. S. D. Druger, M. A. Ratner and A. Nitzam, *Phys. Rev. B* 31 (1985) 3939.
27. T. Miyamoto and K. Shibayama, *J. Appl. Phys.* 44 (1973) 5372.
28. R. Mishra and K. J. Rao, *Solid State Ionics* 106 (1998) 113.
29. J. R. Macdonald, *Impedance spectroscopy*, Wiley, New York (1987).
30. L. M. Hodge, M. D. Ingram and A.R. West, *J. Electroanal. Chem.* 74 (1976) 125.
31. S. L. Agrawal and A. Awadhia, *Bull. Mater. Sci.* 27 (2004) 523.
32. J. R. MacCallum, C. A. Vincent, *Polymer electrolyte review-2* (1997) 43.

33. M. Mudarra, R. D. Calleja, J. Belana, J. C. Can˜adas, J. A. Diego, J. Sellare's and M. J. Sanchi's, *Polymer* 42 (2001) 1647.
34. G. M. Tsangaris, G. C. Psarras and N. Kouloumbi, *J Mater Sci.* 33 (1998) 2027.
35. G. C. Psarras, E. Manolakaki, G. M. Tsangaris, *Composites Part A: Appl Sci Manufact.* 33 (2002) 375.
36. G. M. Tsangaris, N. Kouloumbi and S. Kyvelidis, *Mater Chem Phys.* 44 (1996) 245.
37. T. Furukawa, M. Imura and H. Yuruzume, *Jpn. J. Appl. Physics* 36 (1997) 1119.
38. A. S. Nowick, A. V. Vaysleyb and I. Kuskovsky, *Phys. Rev. B* 58 (1998) 8398.
39. B. Roling, C. Martiny, K. Funke, *J. Non-Crystalline Solids* 249 (1999) 201.
40. C. Cramer, S. Brückner, Y. Gao and K. Funke, *Phys. Chem. Chem. Phys.* 4 (2002), 3214.
41. A. K. Jonscher, *Nature* 267 (1977) 673.
42. K. Funke, *Prog Solid State Chem.* 22 (1993) 111.
43. B. H. Bryskin, Berlin: Verlag Akademie 41 (1985) 169.
44. D. P. Almond, C. C. Hunter and A. R. West, *Materials Science* 19 (1984) 3236.

© 2014 The Authors. Published by ESG ([www.electrochemsci.org](http://www.electrochemsci.org)). This article is an open access article distributed under the terms and conditions of the Creative Commons Attribution license (<http://creativecommons.org/licenses/by/4.0/>).